JPE 18-6-6

https://doi.org/10.6113/JPE.2018.18.6.1659
ISSN(Print): 1598-2092 / ISSN(Online): 2093-4718

Novel Method for Circulating Current Suppression in MMCs Based on Multiple Quasi-PR Controller

Jian Qiu*, Lijun Hang†, Dongliang Liu*, Shengbao Geng**, Xiaonan Ma*, and Zhen Li*

†,*School of Automation, Hangzhou Dianzi University, Hangzhou, China
**Jinan Power Supply Bureau, Jinan, China

Abstract

An improved circulating current suppression control method is proposed in this paper. In the proposed controller, an outer loop of the average capacitor voltage control model is used to balance the sub-module capacitor voltage. Meanwhile, an individual voltage balance controller and an arm voltage balance controller are also used. The DC and harmonic components of the circulating current are separated using a low pass filter. Therefore, a multiple quasi-proportional-resonant (multi-quasi-PR) controller is introduced in the inner loop to eliminate the circulating harmonic current, which mainly contains second-order harmonic but also contains other high-order harmonics. In addition, the parameters of the multi-quasi-PR controller are designed in the discrete domain and an analysis of the stability characteristic is given in this paper. In addition, a simulation model of a three-phase MMC system is built in order to confirm the correctness and superiority of the proposed controller. Finally, experiment results are presented and compared. These results illustrate that the improved control method has good performance in suppressing circulating harmonic current and in balancing the capacitor voltage.

Key words: Capacitor voltage balance, Circulating harmonic current suppression, Discrete domain modeling, Modular multilevel converter (MMC), Multiple quasi-proportional-resonant controller

I. INTRODUCTION

The modular multilevel converter (MMC) is a well-known multilevel topology [1], [2]. It was first introduced in 2001 by R. Marquardt [3]. With the merits of a modular design, low switching frequency, superior harmonic performance, etc. [4]-[6], this topology has been gradually becoming more attractive for the industrial and academic fields, and it has shown more advantages when compared with other converters in a number of areas [7]. By adjusting the number of sub-modules (SMs), a MMC can flexibly adapt to the application of different output voltages or power levels [8-9]. Through continuous development, the MMC has gradually replaced other topologies in medium and high power fields, particularly in high-voltage direct current (HVDC) transmission systems [10]-[13].

In general, the MMC requires a capacitor voltage balancing algorithm [14], [15]. By sorting the SM capacitor voltages and judging the direction of the arm current, [16] and [17] proposed improved selection algorithms to determine the injection or removal of each SM. This method balances the capacitor voltage, and reduces the switching frequency when the number of SMs is large. However, it cannot greatly reduce the switching frequency when the number of SMs is small. The authors of [18] reduced the circulating current through increasing the arm inductance. However, this worsens the system performance by slowing down the frequency response and causing a large voltage drop. The authors of [19] used a double line-frequency, negative-sequence rotational frame to suppress second-order circulating harmonic current by analyzing the harmonic components in the circulating current. However, this method is not feasible when the system is multi-phase. Note that the dominant harmonic component in the circulating current is the double line-frequency. The authors of [20] adopted a notch filter to extract the second-order harmonic. Then they eliminated it by introducing a quasi-proportional-resonant (quasi-PR) controller. However, the calculation burden is

Manuscript received Jul. 17, 2017; accepted Aug. 16, 2018
Recommended for publication by Associate Editor Younghoon Cho.
†Corresponding Author: lijunhang.hhy@aliyun.com
Tel: +86-13957124316, Hangzhou Dianzi University
*School of Automation, Hangzhou Dianzi University, China
**Jinan Power Supply Bureau, China

heavy. By regulating the total capacitor energy and the unbalance energy between the upper and the lower arms within the same leg, the authors of [21] proposed a method to suppress the circulating current by compensating the voltage between the DC-link and every phase. However, this method needs precise information on the angle of the arm equivalent impendence, which slightly affects the performance in practical engineering applications. The authors of [22] presented a multi-resonant strategy to suppress different order circulating harmonic current. However, the proposed strategy decreases the stability margin of the system. In reference [23], a model of the average capacitor voltage control was proposed, which consists of two loops. The outer loop is used for balancing the SM capacitor voltage. The inner loop makes the detected circulating current track the reference provided by the output of the outer loop. This control model is widely used because it suppresses the circulating current and balances the SM capacitor voltage. However, the PI controller used in the inner loop makes it hard to track the reference circulating current without a steady-state error. The authors of [24] replaced the quasi-proportional-resonant controller (PR) of the double line-frequency with a PI controller, where the other high-order frequency harmonics cannot be eliminated.

Based on the model proposed in references [23] and [24], this paper proposes an improved method to suppress circulating current harmonics. First, a mathematical model of a MMC is built. Then the relationship between the average voltages of the SM capacitors and the circulating current is analyzed to indicate that the circulating current contains two parts: the dc component and the harmonics component. Afterwards, by extracting the dc component of the circulating current reference, the harmonics in the circulating current are eliminated by multiple quasi-PR controllers with different resonant frequencies. In addition, in order to better balance the capacitor voltage, an individual voltage balance controller and an arm voltage balance controller are applied in the system. In addition, both the related parameter design methods in the discrete domain and a stability analysis of a multi-quasi-PR controller are given in detail in this paper. Finally, simulation and experimental results are presented to confirm the feasibility and good performance of the proposed control methods.

II. Mathematical Model of a MMC

The circuit of a MMC is shown in Fig. 1, where it has six arms. Each of these arms is constituted by one arm inductor L_0 and N sub-modules (SMs), which are series-connected. The equivalent resistance of each arm is defined as R_0. u_{kp} and u_{kn} (k=a, b, c, and the upper and lower arms are marked as p and n, respectively) are the arm voltages generated by N series-connected SMs. i_{kp} and i_{kn} are the arm currents of phase k and i_{diffk} is the circulating current that flows among the three phases.

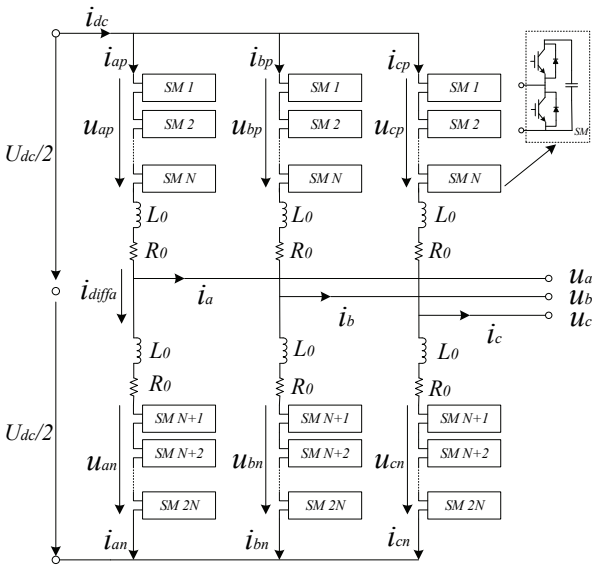

Fig. 1. Diagram of a MMC.

The circulating current can be calculated by the upper arm current and the lower arm current, and is expressed as [25]:

$$i_{diffk} = \frac{i_{kp} + i_{kn}}{2} \tag{1}$$

The mathematical model of a MMC can be summarized as the following equations:

$$u_k = \frac{1}{2}(u_{kn} - u_{kp}) - \frac{1}{2}(L_0 \frac{di_k}{dt} + R_0 i_k) \tag{2}$$

$$2(L_0 \frac{di_{diffk}}{dt} + R_0 i_{diffk}) = U_{dc} - (u_{kn} + u_{kp}) \tag{3}$$

Define e_k as the inner EMF (electromotive force). Then:

$$e_k = \frac{u_{kn} - u_{kp}}{2} \tag{4}$$

The external behavior of a MMC can be described by (2). It can be concluded that the ac network voltage u_k can be regulated by controlling e_k and the two-level converter.

From (3), it is shown that the circulating current i_{diffk} is derived as a mismatch between the sum of the upper and lower arm voltages and the dc-link voltage. Define u_{diffk} as the inner unbalance voltage of phase k, and it can be expressed as:

$$u_{diffk} = L_0 \frac{di_{diffk}}{dt} + R_0 i_{diffk} \tag{5}$$

Apparently, i_{diffk} can be controlled by regulating u_{diffk}. Therefore, the inner characteristic of the MMC can be expressed by Equation (5).

III. Control Strategy for a MMC

Define M as the voltage modulation ratio. Then:

$$M = \frac{E_k}{U_{dc}/2} \tag{6}$$

where, $0 \le M \le 1$. E_k is the magnitude of the inner EMF e_k. The modulation function of the upper and lower arms can be derived as:

$$\begin{cases} m_p = \frac{1}{2}[1 - M\cos(\omega_0 t + \theta)] \\ m_n = \frac{1}{2}[1 + M\cos(\omega_0 t + \theta)] \end{cases} \tag{7}$$

where ω_0 is the fundamental frequency and θ is the initial phase angle.

Equation (7) determines how many sub-modules can be inserted into the arm. Therefore, the number of SMs that should be inserted can be obtained:

$$\begin{cases} N_{up} = m_p * N \\ N_{low} = m_n * N \end{cases} \tag{8}$$

It can be concluded from (8) that the number of SMs inserted into the arm is sinusoidal and that it is in phase with the output voltage. Therefore, the arm current can be decomposed into the sum of the output current i_0 and the circulating current i_{diff} as follows:

$$\begin{cases} i_{kp} = \frac{1}{2} i_0 + i_{diffk} \\ i_{kn} = -\frac{1}{2} i_0 + i_{diffk} \end{cases} \tag{9}$$

Normally, i_{diffk} can be written as equation (10):

$$i_{diffk} = I_{dc} + \sum_{n=2}^{\infty} i_n \tag{10}$$

where n = 2,4,6..., and i_n is the n^{th} harmonic component in the circulating current. This can be expressed as:

$$i_n = I_n * \cos(n\omega_0 t + \gamma_n) \tag{11}$$

According to (11), the circulating current contains the second-order harmonic and other high-order even harmonics.

The sums of the capacitor voltages in the upper arms and lower arms are defined as u_{Ckp} and u_{Ckn}, respectively. In addition, the following equation can be obtained:

$$\begin{cases} C_{SM}\frac{du_{Ckp}}{dt} = C_{SM}\frac{d(\sum u_{Cki})}{dt} = i_{kp}\cdot N \cdot m_p \\ C_{SM}\frac{du_{Ckn}}{dt} = C_{SM}\frac{d(\sum u_{Ckj})}{dt} = i_{kn}\cdot N \cdot m_n \end{cases} \tag{12}$$

where u_{Cki} is the i_{th} (i=1…N) upper arm capacitor voltage in phase k, and u_{Ckj} is the j_{th} (j=N+1…2N) lower arm capacitor voltage in phase k.

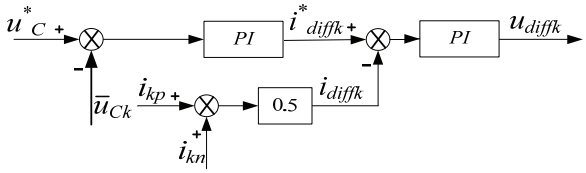

Fig. 2. Control diagram of the traditional control strategy for circulating current suppression.

In the steady state, the sum of all the sub-module capacitor voltages in one phase should be equal to $2U_{dc}$, as shown in the following equation:

$$u_{Cks} = u_{Ckp} + u_{Ckn} = 2U_{dc} \tag{13}$$

According to (12) and (13), the following model can be built:

$$\frac{du_{Cks}}{dt} = \frac{1}{C_{arm}} i_{diffk} - \frac{M}{2C_{arm}} i_k \cdot \cos(\omega_0 t + \theta) \tag{14}$$

Define C_{SM} as the capacitance of the SM capacitor. Thus, the equivalent capacitance of the phase leg can be derived as:

$$C_{arm} = C_{SM}/N \tag{15}$$

Based on (14) and (15), the average SM capacitor voltage of the phase leg k can be expressed as:

$$\bar{u}_{Cks} = \frac{1}{C_{arm}} I_{diffk} + \frac{M}{2C_{arm}T}\int_0^T i_k \cdot \cos(\omega_0 t + \theta) dt \tag{16}$$

where T is the switch period, and I_{diffk} is the dc component of the circulating current. It can be concluded that the dc component of the circulating current determines the balance of the SM capacitor voltage in each phase.

A. Traditional Control Strategy for Circulating Current Suppression of a MMC

The authors of [23] proposed a model of an average capacitor voltage control which has been widely used in MMCs under a modulation mode called CPS-PWM.

A control diagram of this model is shown as Fig. 2. It can be seen that the outer loop forces the average capacitor voltage $\bar{u}_{ck}$ to track its reference value u^*_c, and through the PI controller, it generates the circulating current reference i^*_{diffk}. The inner loop outputs the unbalance voltage u_{diffk}, which can be obtained by making the actual circulating current i_{diffk} follow i^*_{diffk} to compensate the difference between the dc-link voltage and the phase leg voltage. The average capacitor voltage $\bar{u}_{ck}$ can be calculated by equation (17):

$$\bar{u}_{Ck} = \frac{1}{2N}\left(\sum_{i=1}^{N} u_{Cki} + \sum_{j=N+1}^{2N} u_{Ckj}\right) \tag{17}$$

The circulating current is mainly composed of a dc component, second-order harmonic component and other high-order harmonic components. Therefore, the difference between i^*_{diffk} and i_{diffk} has a lot of harmonic components.

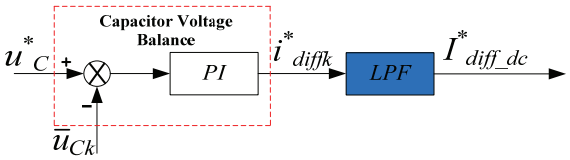

Fig. 3. Diagram of dc component extraction.

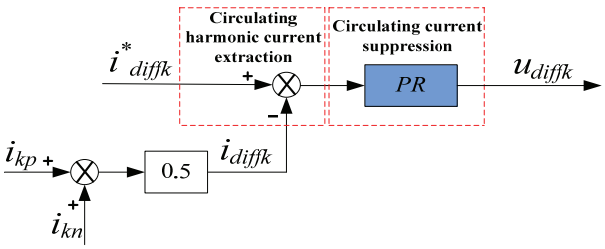

Fig. 4. Diagram of a control strategy for circulating current suppression using a quadratic-resonant quasi-PR controller.

However, the PI controller used in the inner loop can eliminate static errors when tracking the dc component. However, it cannot track the ac component without a static error. Therefore, this model performs well in balancing the SM capacitor voltage. However, it cannot suppress the circulating current completely. Although the harmonic components of the circulating current only flow between three phases without affecting the output current, they distort the arm currents, increase system loss and deteriorate the system performance.

B. Improved Control Strategy for Circulating Current Suppression of a MMC

In order to improve the quality of the arm current, decrease the system loss and enhance the system performance, the authors of [24] proposed an improved control strategy to further suppress circulating current. First, based on an analysis of the aforementioned average voltage model, it is necessary to eliminate the second order component from the output of the voltage loop in order to suppress the circulating current harmonics. Therefore, a low-pass filter is proposed to extract the dc component from the outer loop output in Fig. 2, as shown as Fig. 3 [24].

To reduce the order of the system and simplify the system design, a first-order low-pass filter is used in the controller and its transfer function is given by:

$$F(s)=\frac{1}{s\cdot T_s+1} \tag{18}$$

where T_s is the time constant, and the cut-off frequency of this filter is $1/(2\pi/T_s)$.

Afterwards, the circulating current harmonics are separated from the circulating current reference, which contains the second-order harmonic and other high-order even harmonics. Among them, the second-order harmonic is the main component. In the other harmonics, the four-order harmonic, six-order harmonic and eight-order harmonic are the dominating ones. The authors of [24] proposed a second- order quasi-PR controller to eliminate the second-order harmonic from circulating current as shown in Fig. 4. However, the quadratic-resonant quasi-PR controller cannot eliminate other harmonics in the circulating current. In order to further eliminate the other order harmonics, an improved control strategy for the circulating current has been proposed. This method uses a multi-quasi-PR controller to suppress the second-order harmonic and other high-order harmonics as shown in Fig. 5.

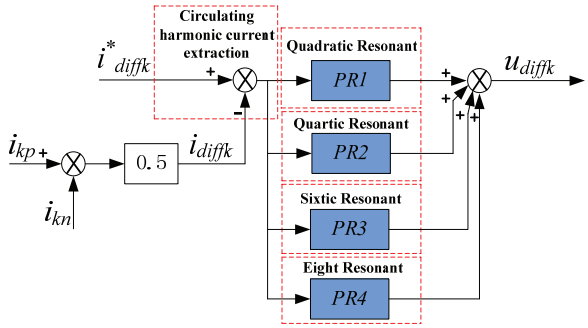

Fig. 5. Diagram of the improved control strategy for circulating current suppression using multiple quasi-PR controllers.

The transfer function of the multiple quasi-PR is written as:

$$F_{PR}(s)=K_p+\sum_{n=2,4,6...}\frac{2K_{rn}\omega_{cn}s}{s^2+2\omega_{cn}s+(n\omega_0)^2} \tag{19}$$

where K_p and K_{rn} are the scale coefficient and resonance gain of the controller, respectively. ω_{cn} is the response bandwidth used to decrease the sensitivity of the resonant controller when a frequency shift occurs, and ω_0 is the fundamental angular frequency. Because the second-order harmonic, fourth-order harmonic, sixth-order harmonic and eighth-order harmonic are major parts of the circulating current harmonic, n can be set to 2, 4, 6 and 8 in equation (19). Thus, it can be seen from Fig. 5 that there is a quadratic quasi-PR controller, quartic quasi-PR controller, sixth quasi-PR controller and eighth quasi-PR controller in the multi-quasi-PR controller. These four controllers are added in parallel to get u_{diffk}.

A bode diagram of the quasi-PR controllers introduced in Fig. 5 is shown in Fig. 6. Here the parameters of the controller are selected as: K_p = 10, K_{rn} = 1200, $\omega_{cn}=1.5$ rad/s and $\omega_0=100\pi$ rad/s. Since these parameters influence the stability and dynamic response of the system, they should be designed carefully. The detailed process of parameter designing will be introduced in the next section.

It can be seen from the magnitude diagram in Fig. 6 that the magnitude curve has four resonance peaks at four frequency points ω_0, $2\omega_0$, $3\omega_0$ and $4\omega_0$, respectively. This

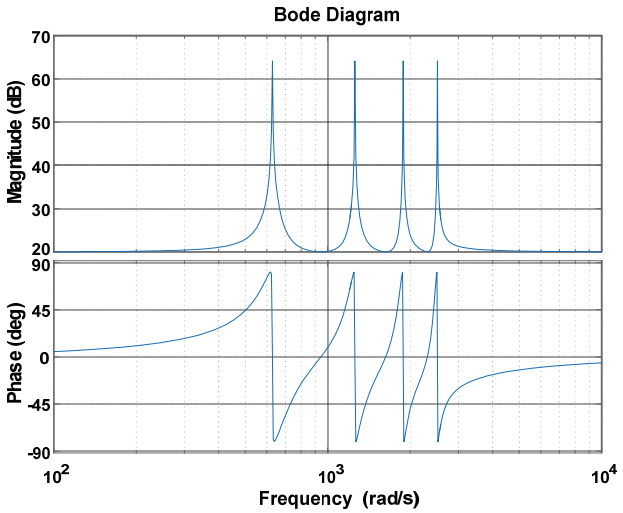

Fig. 6. Bode diagram of a multiple quasi-PR controller.

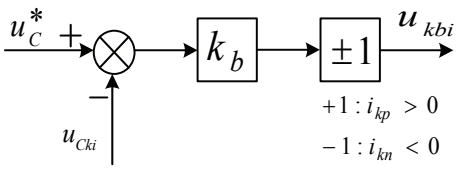

Fig. 7. Diagram of the individual balance controller for each SM.

can suppress the circulating current with a relative frequency. However, it can also be seen from phase diagram in Fig. 6 that the phase curve changes dramatically at the resonance peak, which may reduce the phase margin of the system. Therefore, the control parameters should be selected properly to prevent system instability.

From the above analysis, the arm voltage references of phase *k* can be given as:

$$\begin{cases} u_{kp}^{*} = \dfrac{1}{2}U_{dc} - e_k - u_{diffk} \\ u_{kn}^{*} = \dfrac{1}{2}U_{dc} + e_k - u_{diffk} \end{cases} \tag{20}$$

Under the CPS-PWM method, the arm voltage reference is averagely assigned to *N* SMs. Therefore, the *N* SMs are all in the switching on and off state. Thus, every SM is modulated depending on its own carrier wave and modulation wave. Then the individual voltage balance controller can be applied to regulate the modulation carrier, as shown in Fig.7. A detailed description can be found in [23], [24].

According to Fig. 5 and Fig. 7, the voltage reference of the i_{th} SM in phase *k* u_{kpi} can be calculated as in (21):

$$u_{kpi} = u_{kp}^{*} + u_{kbi} \tag{21}$$

By combing (19), (20) and (21), the circulating current suppressing and capacitance voltage balancing can be achieved.

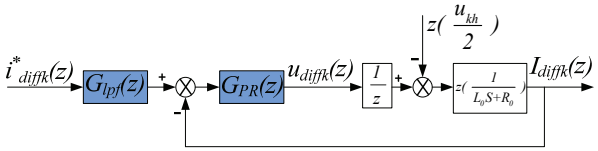

Fig. 8. Diagram of a circulating current suppression model.

IV. Principles of the Parameters Design

The principles of the parameter design for a multi-quasi-PR controller in discrete domain are given in this section.

As discussed in Section II, it is the inner unbalance voltage u_{diffk} that regulate the circulating current i_{diffk}. Therefore, the circulating current suppression model can be modified as shown in Fig. 8 according to the controllers described in Fig. 3 and Fig. 4, where u_{kh} is the equivalent harmonic voltage source in phase *k* (refer to [25] for a more detailed analysis).

Define $G_s(z)=Z(1/(L_0s+R_0))$. Then the expression of the circulating current and its error can be written as (22) and (23):

$$i_{diffk}(z) = \frac{G_{pr}(z)G_s(z)z^{-1}}{1+G_{pr}(z)G_s(z)z^{-1}} \cdot (G_{lpf}(z)i_{diffk}^{*}(z)) - \frac{G_s(z)}{1+G_{pr}(z)G_s(z)z^{-1}} \cdot \frac{u_{kh}(z)}{2} \tag{22}$$

$$e(z) = \frac{G_{lpf}(z)i_{diffk}^{*}(z) + G_s\dfrac{u_{kh}(z)}{2}}{1+G_{pr}G_s z^{-1}} \tag{23}$$

The control system needs to make the circulating current i_{diffk} follow its reference command and minimize the error caused by the disturbance. The low-pass filter (LPF) in Fig. 6 acts as a forward feedback to eliminate the second-order harmonic component in i^{*}_{diffk}. The cutoff frequency of the LPF is set to 20Hz for better extrication of the dc component and filtering of the second-order harmonic component. By using a Tustin transformation, the transfer function of a LPF in the z-domain, can be written as:

$$G_{lpf}(z) = \frac{0.0141(z+1)}{z-0.9718} \tag{24}$$

Considering the actual grid fluctuations, if the grid frequency ripple is (50±0.5) Hz, then ω_0 in (19) should be selected as 100π rad/s. In addition, $\omega_{cn}=(n\pi)$ rad/s and n = 2,4,6,8. Employing a Tustin transformation, the z-domain form of the multiple quasi-PR can be obtained in (25):

$$G_{pr}(z) = K_p + \frac{A_2(z^2-1)}{z^2-1.982z+0.9975} + \frac{A_4(z^2-1)}{z^2-1.933z+0.9951} + \frac{A_6(z^2-1)}{z^2-1.856z+0.9927} + \frac{A_8(z^2-1)}{z^2-1.754z+0.9906} \tag{25}$$

The expression of A_n(n=2, 4, 6, 8) can be given as:

$$A_n = \frac{K_{rn}\omega_{cn}T_s}{1+\omega_{cn}T_s+(\omega_0 T_s)^2} \tag{26}$$

where K_{rn} is defined as the resonance gain, T_s is the sampling period.

In experimentation, the arm inductance L_0 is equal to 5mH, and its equivalent resistance is assumed to be $0.5\,\Omega$. By applying a ZOH transformation, the impedance transfer function can be derived as (27):

$$G(z) = \frac{0.0396}{z-0.9802} \tag{27}$$

Considering the action of a disturbance, the system response should tend to be zero, and the error equation is given by (28):

$$E_h(z) = 0 - i_{diffk}(z) = \frac{G_s(z)}{1+G_{pr}(z)G_s(z)z^{-1}} \cdot \frac{u_{kh}}{2}(z) \tag{28}$$

Then, under a unit step disturbance, the steady state error can be written as (29):

$$\lim_{n\to 1}(1-z^{-1})E_h(z) = \frac{2}{1+2K_p} \tag{29}$$

If the relative error is required to be less than 0.1, then $K_p > 9.5$. Based on (25), (26), (27) and (28), the open-loop transfer function can be written as (30):

$$G_0(z) = \frac{0.0396}{z(z-0.9802)} G_{pr}(z) \tag{30}$$

The value of A_n in $G_{pr}(z)$ is significant to the controller because it directly affects the circulating current suppression and the system stability. In order to facilitate the analysis, A_2, A_4, A_6 and A_8 become the same in the controller. It is verified that the system is stable when using the same value for A_2, A_4, A_6 and A_8.

According to (30), Fig. 9 shows a bode diagram of the open-loop system with the variation of A_n when K_p = 12. It can be seen from Fig. 9 that the open-loop magnitude curve has four resonance peaks. In addition, the magnitude around the resonance frequency points increases with A_n, which means that the multiple quasi-PR controller has better performance when A_n increases. However, with an increase of A_n, the phase lag around the resonant frequency also increases, which reduces the phase margin of the system.

Fig. 10 shows a bode diagram of the open-loop system with the variation of K_p when A_n= 0.12. It can be seen from Fig. 10 that the open-loop gain at the point of the resonant frequency of the system increases with K_p, which is helpful for circulating current suppression. In addition, when K_p increases, the steady precision of the system is improved. However, the magnitude margin and the phase margin of the system is reduced, which is not beneficial to the stability of the system.

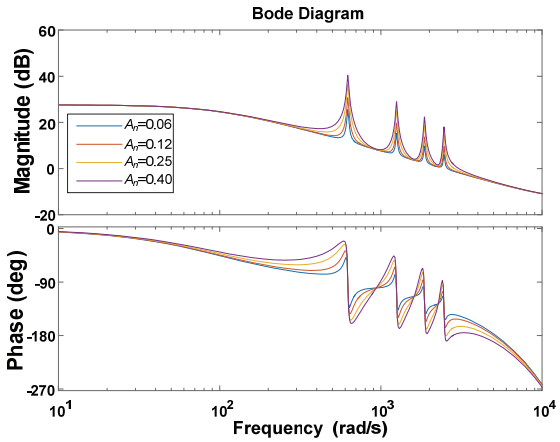

Fig. 9. Bode diagram of the open-loop system with variations of A_n(K_p = 12).

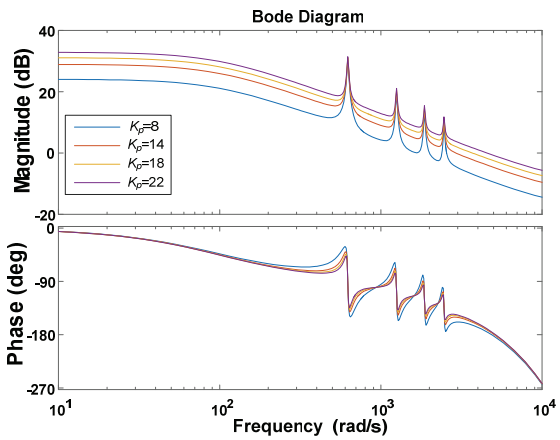

Fig. 10. Bode diagram of the open-loop system with variations of K_p(A_n=0.12).

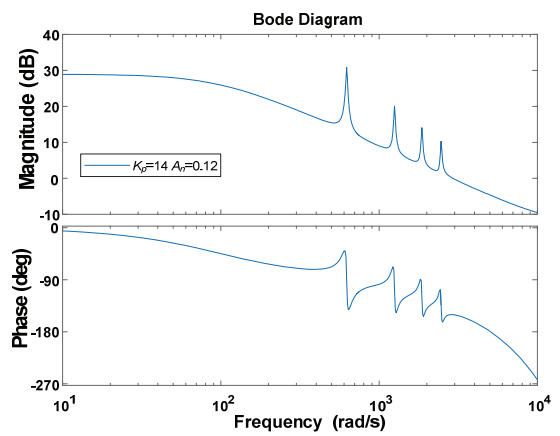

Fig. 11. Bode diagram of the open-loop system with the parameters K_p = 14 and A_n= 0.12.

Considering the performance of the circulating current suppression and the stability of the system, the parameters are selected as: K_p = 14 and A_n = 0.12. Fig. 11 shows a bode diagram of the open-loop system with the selected parameters. It can be seen that the magnitude margin and phase margin are 4.7dB and 30°, respectively. This indicates that the

TABLE I
MAIN CIRCUIT PARAMETERS OF THE MMC IN THE SIMULATION

Items	Symbol	Value
Number SMs per arm	N	4
Arm inductance	L_0/mH	5
Sub-module capacitance	C/mF	1
DC supply voltage	U_{dc}/V	680
Sub-module capacitor voltage	U_{Cki}/V	170
Output RMS voltage	u_{ab}/V	381
Output RMS current	I_k/A	8.8
Output inductance	L_f/mH	4
Output frequency	f_0/Hz	50
Rated load	R_0/Ω	25

system is stable.

It is noteworthy that when compared with a quadratic quasi-PR controller, the multi-quasi-PR controller has less magnitude margin and phase margin due to the presence of multiple resonance peaks.

V. SIMULATION RESULTS

To verify the correctness and effectiveness of the improved method proposed in this paper, a simulation model for a MMC system of three phases with a passive load was built using MATLAB/Simulink. The main circuit parameters in the system are listed in Table I. First, the traditional control strategy is applied in the simulation. Then the improved control strategy is used in the simulation to make a comparison with the traditional control strategy.

A. The PI Control Strategy Application in the Simulation

By applying a PI control strategy in the circulating current suppression, the simulation results are shown in Fig. 12. Fig. 12(a) gives the phase voltage of the passive loads. The upper and lower arm currents of phase *A* are shown in Fig. 12(b). Fig. 12(c) gives the circulating current i_{diffa} and its peak-peak value, which is about 1.5A. Therefore, the PI control strategy has a limited ability to suppress circulating current.

B. The Quadratic quasi-PR Control Strategy Application in Simulation

Since the traditional PI controller cannot suppress the second order harmonic in the circulating current, the quadratic quasi-PR controller can be applied. Fig. 13 shows the main harmonics of the circulating current in phase *A* after using the quadratic quasi-PR control and the traditional PI control, respectively. As shown in Fig. 13, when the quadratic quasi-PR control is applied, the second order harmonic in the circulating current is rapidly suppressed when compared with traditional PI control. As a result, the amplitude of the circulating current is reduced.

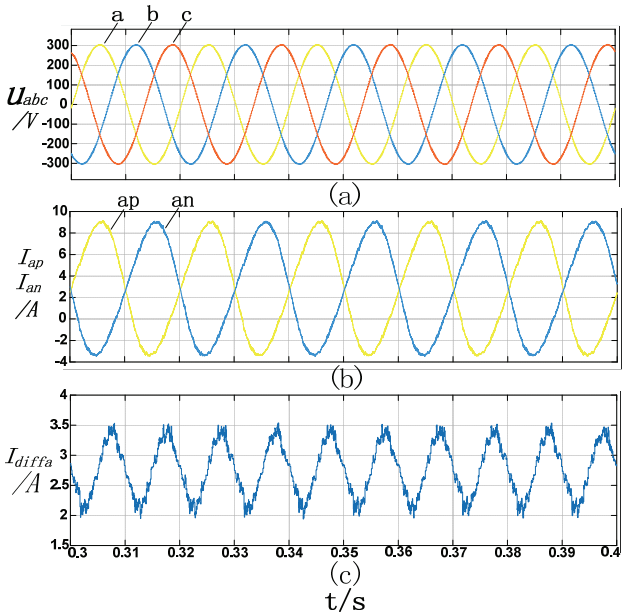

Fig. 12. Simulation results of a MMC when using the PI control strategy.

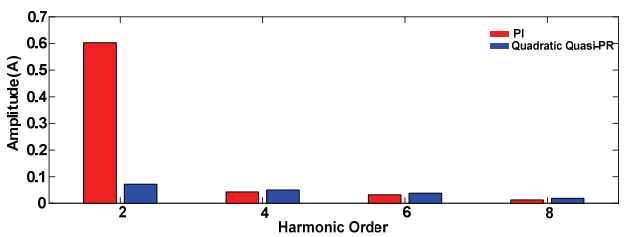

Fig. 13. Main harmonics of the phase *A* circulating current in simulations using the quadratic quasi-PR control and the PI control.

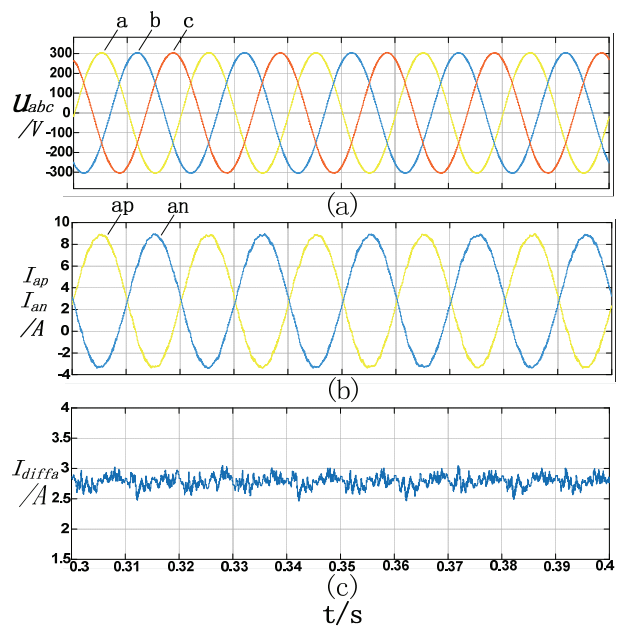

Fig. 14. Simulation results of a MMC when using the multiple quasi-PR control strategy.

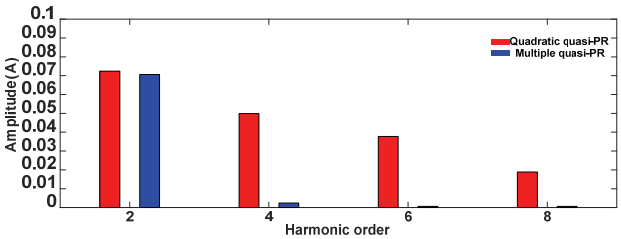

Fig. 15. Main harmonics of the phase *A* circulating current in simulations using the quadratic quasi-PR control and the multi-quasi-PR control.

C. The multi-quasi-PR Control Strategy Application in Simulation

Applying the multi-quasi-PR control strategy, the obtained simulation results are shown as Fig. 14.

Fig. 14 shows that quadratic quasi-PR control has good ability to suppress the second order harmonic in the circulating current. In order to verify that multi-quasi-PR controller has the ability to suppress the high order harmonics in the circulating current, Fig. 15 shows the main harmonics of the circulating current in phase *A* after using the quadratic quasi-PR control and the multi-quasi-PR control, respectively. As shown in Fig. 15, when the quadratic quasi-PR control is used, the other high order harmonics in the circulating current still exist apart from the second order harmonics. However, the multi-quasi-PR control can suppress the second order harmonic in the circulating current, and the other main high order harmonics, which verifies the effectiveness of the proposed controller.

VI. Experiment Results

In order to verify the effectiveness of the multi-quasi-PR controller proposed in this paper, a three phase MMC prototype with a passive load was built. The hardware platform is shown in Fig. 16. In the experimental platform, a TMS320F28335 from TI and a FPGA EP3C16Q240C8 from ALTERA are selected as the control units. In addition, an IGBT FGA180N30D from FAIRCHILD is selected as the switching device, and the material of inductor used in the circuit is FeSiAl.

The main circuit parameters of the experimental platform are shown in Table II. In this experiment, three control strategies for circulating current suppression will be compared, including PI control, quadratic quasi-PR control and multiple quasi-PR control. In addition, the three-phase output voltage, the arm current in phase *A* and the circulating current in phase *A* of each control strategy will be shown. The main parameters of the three control strategies are shown in Table III according to the analysis in section IV.

A. The PI Control Strategy Applied in the Experiment

After applying the PI control strategy, experimental results

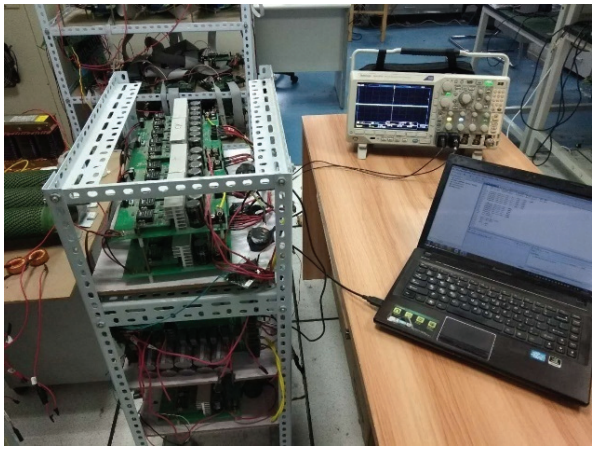

Fig. 16. Practical hardware platform of a MMC.

TABLE II
Main Circuit Parameters of the MMC in the Experiment

Items	Symbol	Value
Number SMs per arm	N	4
Arm inductance	L_0/mH	5
Sub-module capacitance	C/mF	1.3
DC supply voltage	U_{dc}/V	300
Sub-module capacitor voltage	U_{Cki}/V	75
Output RMS voltage	u_{ab}/V	163
Output RMS current	I_k/A	3.75
Output inductance	L_f/mH	4
Output frequency	f_0/Hz	50
Rated load	R_0/Ω	25

TABLE III
Main Control Parameters in the Experiment

Control Strategy	Control Parameters
PI	$K_p = 14$ $K_i = 200$
Quadratic quasi-PR	$K_p = 14$ $A_n = 0.12$
Multiple quasi-PR	$K_p = 14$ $A_n = 0.12$

are shown in Fig. 17. Fig. 17(a) gives the three-phase output voltage. The upper and lower arm currents of phase *A* are shown in Fig. 17(b). When compared with a standard sinewave, the current waves are distorted due to the presence of circulating current. Fig. 17(c) gives the circulating current i_{diffa} and the peak-peak value is about 1.2A. In addition, it can be seen from Fig. 17(c) that there is an obvious second harmonic in the circulating current.

B. The Quadratic Quasi-PR Control Strategy Applied in the Experiment

After applying the quadratic control strategy, experimental results are shown in Fig. 18.

Comparing Fig. 18(b) with Fig. 17(b), it can be seen that

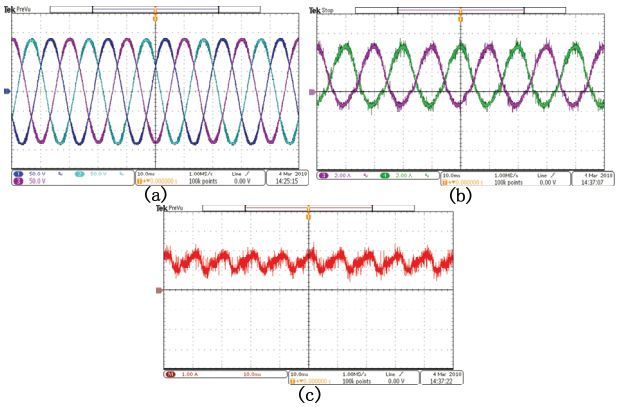

Fig. 17. Experimental results of the PI control.

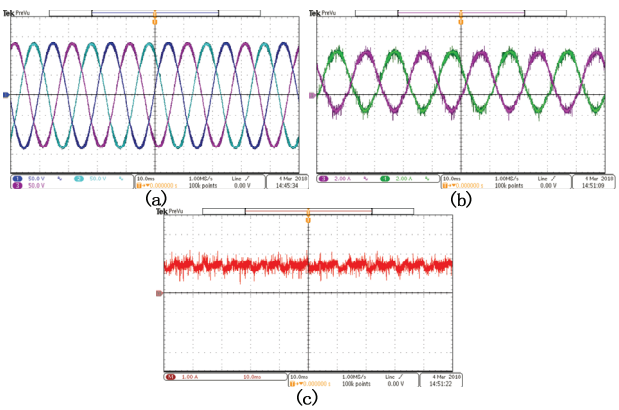

Fig. 18. Experimental results of the quadratic quasi-PR control.

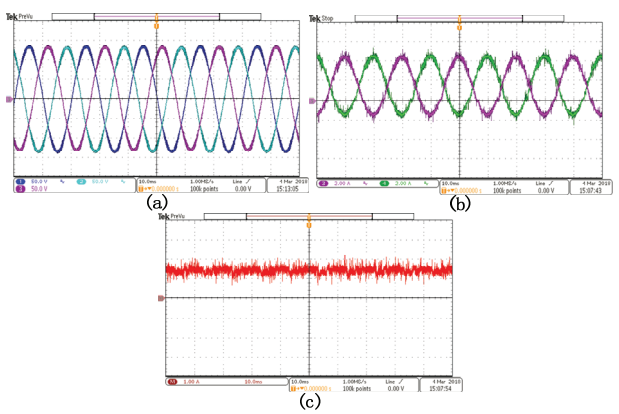

Fig. 19. Experimental results of the multiple quasi-PR control.

the sine quality of the arm current has been improved. In addition, comparing Fig. 18(c) with Fig. 17(c), it can be seen that the peak-peak value of the circulating current is reduced to about 0.8A after the quadratic quasi-PR control is applied. In addition, the second order harmonic in the circulating current has been obviously suppressed.

C. The Multiple Quasi-PR Control Strategy Applied in the Experiment

After applying the quadratic control strategy, experimental results are shown in Fig. 19.

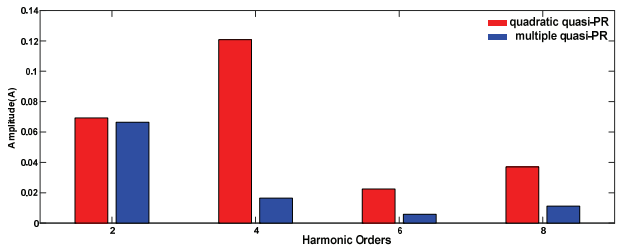

Fig. 20. Main harmonics of the phase A circulating current in the experiment.

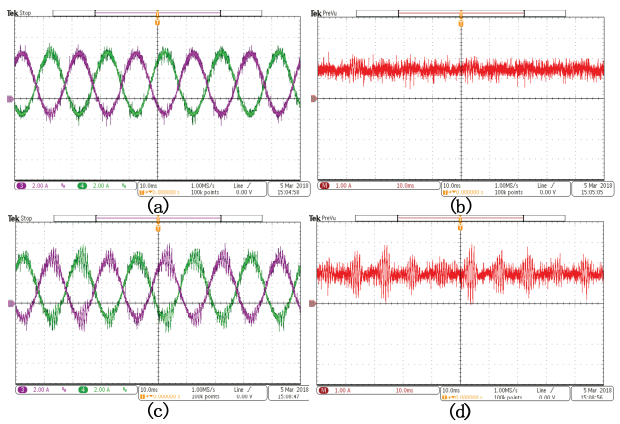

Fig. 21. Arm current and circulating current with an increase of K_p ($A_n = 0.12$).

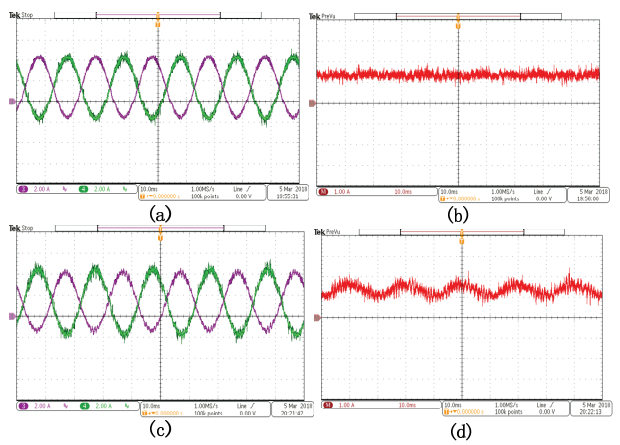

Fig. 22. Arm current and circulating current with an increase of A_n($K_p = 0.14$).

From Fig. 19(b), it can be seen that the arm current still has a good sine quality. In addition, it can be concluded from Fig. 19(c) that the multi-quasi-PR controller still has a good ability to suppress circulating current, and the system is stable under the selected control parameters.

In order to verify that the multi-quasi-PR controller has the ability to suppress the high order harmonics in the circulating current when compared with the quadratic quasi-PR controller, the main harmonics of the circulating current in phase A after using the quadratic quasi-PR control and the multi-quasi-PR control are shown in Fig. 20.

As shown in Fig. 20, the other high order harmonics in the circulating current are relatively large apart from the second order harmonics when the quadratic quasi-PR control is used. However, after using the multi-quasi-PR control, the second order harmonic in the circulating current is suppressed, and the other main high order harmonics are greatly reduced.

In this experiment, since the power of system is not very large, the advantages of the multi-quasi-PR controller are not obvious. However, the system power is great in practical MMC applications that cause a large circulating current. In this case, the advantages of the proposed control strategy will be clearly represented.

The parameters of the multi-quasi-PR controller used in the experiment are shown in Table III. Now keep the parameter A_n unchanged, and increase the parameter K_p. Fig. 21(a) and (b) show the arm current and circulating current in phase A when K_p = 18. It can be seen that the arm current starts to jitter. K_p is further increased to 24, and the results are shown in Fig. 21(c) and (d). It seems that when K_p = 24, the arm current oscillates. Thus, when K_p increases, the stability of the system deteriorates, which is the same as the analysis of section IV.

A similar analysis can be done when A_n increases, while K_p is unchanged. When A_n = 0.3, the arm and circulating current in phase A are shown in Fig. 22(a) and (b) respectively. Increase A_n, and the results are shown in Fig. 22(c) and (d). It can be concluded that with an increase of A_n, the oscillation of the arm current is more obvious, which means that the stability margin of the system is reduced.

VII. CONCLUSIONS

A novel controller to suppress circulating current harmonics is proposed in this paper. When compared with the traditional control strategy for circulating current suppression, the control loop is improved by adding a dc component extraction unit and a multi-quasi-PR controller. In addition, an individual capacitor voltage balancing control is applied to balance the capacitor voltage in the SM. Furthermore, the parameter design principles of the multi-quasi-PR controller are proposed in the discrete-domain for obtaining better effectiveness, and the stability of the system is also analyzed. In order to confirm the correctness and superiority of the improved control method, a simulation model is built. Finally, a comparison of experimental results before and after the improvement verifies the feasibility and effectiveness of the improved control method.

ACKNOWLEDGMENT

This paper is supported by the National Natural Science Foundation of China (NSFC) (Grant No.51777049, No.51707051).

REFERENCES

[1] J. Kucka, D. Karwatzki, L. Baruschka, and A. Mertens, "Modular multilevel converter with magnetically coupled branch inductors," *IEEE Trans. Power Electron*., Vol. 32, No. 9, pp. 6767-6777, Sep. 2017.

[2] P. T. Lewis, B. M. Grainger, H. A. AI Hassan, A. Barchowsky, and G. F. Reed, "Fault section identification protection algorithm for modular multilevel converter-based high voltage DC with a hybrid transmission corridor," *IEEE Trans. Ind. Electron*., Vol. 63, No. 9, pp. 5652-5662, Sep. 2016.

[3] J. Rodriguez, J.-S Lai, and Z. Fang, "Multilevel inverters: a survey of topologies, controls, and applications," *IEEE Trans. Ind. Electron*., Vol. 49, No. 4, pp. 724-738, Aug. 2002.

[4] S. Debnath, J. Qin, B. Bahrani, and M. Saeedifard. "Operation, control, and applications of the modular multilevel converter: A review," *IEEE Trans. Power Electron*., Vol. 30, No. 1, pp. 37-53, Jan. 2015.

[5] L. Harnefors, A. Antonopoulos, S. Norrga, and L. Angquist, "Dynamic analysis of modular multilevel converters," *IEEE Trans. Ind. Electron*., Vol. 60, No. 7, pp. 2526-2537, Jul. 2013.

[6] D. Siemaszko, A. Antonopoulos, K. V, M. Vasiladiotis, L. Angquist, and H.-P. Lennart, "Evaluation of control and modulation methods for modular multilevel converters," in *Proc. Int. Power Electro. Conf*., pp. 746-753, Jun. 2010.

[7] M. Espinoza, R. C´ardenas, M. D´ıaz, and J. C. Clare, "An enhanced dq-based vector control system for modular multilevel converters feeding variable-speed drives," *IEEE Trans. Ind. Election*., Vol. 64, No. 4, pp. 2620-2630, Apr. 2017.

[8] A. Legnica and R. Marquardt, "An innovative modular multilevel converter topology suitable for a wide power range," *Power Tech. Conf. Proc*., pp. 23-26, Jun. 2003.

[9] D. Siemaszko, A. Antonopoulos, K. Ilves, M. Vasiladiotis, L. Angquist, and H.-P. Nee, "Evaluation of control and modulation methods for modular multilevel converters," *Int. Power Elec. Conf.*, pp. 21-24, Jun. 2010.

[10] H. Liu, L. Poh, and F. Blaabjerg, "Generalized modular multilevel converter and modulation," *Int. Power Elec. Conf.*, pp. 2034-2038, May. 2014.

[11] I. A. Gowaid, G. P. Adam, S. Ahmed, D. Holliday, and B.W. Williams, "Analysis and design of a modular multilevel converter with trapezoidal modulation for medium and high voltage DC-DC transformers," *IEEE Trans. Power Electron*., Vol. 20, No. 10, pp. 5439-5457, May 2015.

[12] A. Nami, J. Liang, F. Dijkhuizen, and G. D. Demetriades, "Modular multilevel converters for HVDC applications: Review on converter cells and functionalities," *IEEE Trans. Power Electron*., Vol. 30, No. 1, pp. 18-36, Jan. 2015.

[13] B. Li, S. Zhou, D. Xu, R. Yang, D. Xu, C. Buccella, and C. Cecati, "An improved circulating current injection method for modular multilevel converters in variable-speed drives," *IEEE Trans. Ind. Electron*., Vol. 63, No. 11, pp. 7215-7225, Mar. 2016.

[14] F. Hahn, M. Andresen, G. Buticchi, and M. Liserre, "Thermal analysis and balancing for modular multilevel converters in HVDC applications," *IEEE Trans. Power Electron*., Vol. 33, No. 3, pp. 1985-1996, Mar. 2018.

[15] Y. Tang, L. Ran, O. Alatise, and P. Mawby, "Capacitor selection for modular multilevel converter," *IEEE Trans. Ind. Appl*., Vol. 52, No. 4, pp. 3279-3293, Jul./Aug. 2016.
[16] M. Moranchel, E. J. Bueno, F. J. Rodriguez, and I. Sanz, "Novel capacitor voltage balancing algorithm for modular multilevel converter," *Ann. Conf. Ind. Electron. Society*, pp. 4697-4701, Oct. 2014.
[17] S. Rohner, S. Bernet, M. Hiller, and R. Sommer, "Modulation, losses and semiconductor requirement of modular multilevel converters," *IEEE Trans. Ind. Electron*., Vol. 57, No. 8, pp. 2633-2642, Aug. 2010.
[18] Q. Tu, Z. Xu, H. Huang, and J. Zhang, "Parameters design principles of the arm inductor in modular multilevel converter based HVDC," *Proc. Int. Conf. Power Syst. Technol*., pp. 1-6, 2010.
[19] Q. Tu, Z. Xu, and L. Xu, "Reduced switching-frequency modulation and circulating current suppression for modular multilevel converters," *IEEE Trans. Power Del*., Vol. 26, No. 3, pp. 2009-2016, Jul. 2011.
[20] F. Yan, G. Tang, Z. He, M. Kong, and W. Ma, "A novel circulating current controller for modular multilevel converter," *Automation of Electric Power Systems*, Vol. 38, No.1, pp. 104-108, Jan. 2014.
[21] A. Antonopoulos, L. Angquist, and H.-P. Nee, "On dynamics and voltage control of the Modular Multilevel Converter," *Eur. Conf. Power Electron. Appl*., pp. 1-10, Sep. 2009.
[22] J. Gao, J. Su, H. Gao, Y. Ding, and J. Wang. "Capacitor voltage and circulation current control strategy in modular multilevel converter," Power System Protection and Control, Vol. 42, No.3, pp. 56-62, Feb. 2014.
[23] M. Hagiwara and H. Akagi. "Control and experiment of pulsewidth-modulated modular multilevel converters," *IEEE Trans. Power Electron*., Vol. 24, No. 7, pp. 1737-1746, Jul. 2009.
[24] S. Geng, Y. Gan, Y. Li, L. Hang, and G. Li, "Novel circulating current suppression strategy for MMC based on quasi-PR controller," *IEEE Applied Power Electronics Conference and Exposition (APEC)*, pp. 3560-3565, 2016.
[25] M. Zhang, L. Huang, W. Yao, and Z. Lu, "Circulating harmonic current elimination of a CPS-PWM based modular multilevel converter with a Plug-In repetitive controller," *IEEE Trans. Power Electron*., Vol. 29, No. 9, pp. 2083-2097, Apr. 2009.

Jian Qiu was born in Ningbo, China. He received his B.S. degree in Automation from the Northeast University at Qinhuangdao, Qinhuangdao, China, in 2016. He is presently working towards his M.S. degree in Electrical Engineering from Hangzhou Dianzi University, Hangzhou, China. His current research interests include power electronic digital control, modular multilevel converters and ac machine drives.

Lijun Hang (M'09) received her B.S. and Ph.D. degrees in Electrical Engineering from Zhejiang University, Hangzhou, China, in 2002 and 2008, respectively. From 2008 to 2011, she was a Postdoctoral Researcher at Zhejiang University. From 2011 to September 2013, she was a Research Assistant Professor in CURENT, University of Tennessee, Knoxville, TN, USA. She is presently working as a Professor in the Department of Electrical Engineering, Hangzhou Dianzi University, Hangzhou, China. She has authored or co-authored more than 80 technical papers published in journals and conference proceedings. Her current research interests include digital control of power electronics for grid connected converters, converters for microgrids, and renewable energy.

Dongliang Liu was born in Zhangjiagang, China. He received his Ph.D. degree in Control Theory and Control Engineering from Zhejiang University in 2005. He was engaged in research on AC servo motor and control in the postdoctoral workstation of Wolong Holding Group from 2005 to 2007. His current research interests include nonlinear control strategies, permanent magnet AC servo drive control systems, electric vehicle electric drive systems, new energy sources and related power electronics applications.

Shengbao Geng was born in Liaocheng, China. He received his B.S. degree in Electrical Engineering from the Shanxi University of Science and Technology, Xi'an, China, in 2013; and his M.S. degree in Electrical Engineering from Shanghai Jiao Tong University, Shanghai, China, in 2016. He is presently working in the Jinan Power Supply Bureau, Jinan, China. His current research interests include cable installation, cable operation and state maintenance of electrical equipment.

Xiaonan Ma was born in Jinzhou, China. She received her B.S. degree in Electrical Engineering from Hangzhou Dianzi University, Hangzhou, China, in 2016, where she is presently working towards her M.S. degree in Electrical Engineering. Her current research interests include power electronic digital control, high power AC-DC converters and dual active bridge converters.

Zhen Li was born in Suqian, China. He received his B.S. degree in Automation from the Nanjing University of Technology, Nanjing, China, in 2016. He is presently working towards his M.S. degree in Electrical Engineering from Hangzhou Dianzi University, Hangzhou, China. His current research interests include power electronic digital control, testing of power devices and high-power DC-DC converters.